Preprints of the 19th World Congress
The International Federation of Automatic Control
Cape Town, South Africa. August 24-29, 2014

Non-linear model-based Control for the Human-inspired Robotic Exoskeleton (HuREx) gait trainer

Kazuto Kora* Andrew McDaid **
Sheng Xie***

**Department of Mechanical Engineering, The University of Auckland*
Auckland, New Zealand, (e-mail: kkor008@aucklanduni.ac.nz).
*** (e-mail:andrew.mcdaid@auckland.ac.nz)*
****(e-mail:s.xie@auckland.ac.nz)*

Abstract: A non-linear model-based control system for the Human inspired Robotic Exoskeleton (HuREx) gait trainer was developed. The model used for the controller was derived using a hybrid PMA model and dynamic model of the device. The performance of the control system was compared against a closed-loop PID control system in simulation. The trajectory tracking results show that the model-based control system improved the speed and accuracy of the system as well as being robust against modeling errors and disturbances.

Keywords: Nonlinear control, Model-based control, Modelling, Robotics, Simulation, Impedance control, Rehabilitation, Gait

1. INTRODUCTION

Physical rehabilitation is time consuming and labour intensive for both patients and therapists. Robotic rehabilitation has been introduced over the past years to reduce the work load as well as provide more repeatable and consistent therapy to patients over a long period of time. With advances in robot actuation and exoskeleton design, robot aided rehabilitation has the potential to result in lower health care costs for therapy as well as much improved patient outcomes. This is extremely important as stroke is one of the main causes of adult disability and has among the highest cost of hospitalization with fewer than 50% of patients regaining their independence after 6 months (Wade and Hewer, 1987). Using traditional therapy the small gains in walking quality and speed following stroke prevents many patients from becoming community walkers (Perry et al., 1995, Tilson et al., 2010).

There have been a number of devices developed for lower limb gait training, including exoskeleton devices such as the Lokomat (Riener et al., 2005), LOPES (Veneman et al., 2007) and the AutoAmbulator (HealthSouth). A detailed review of these devices is given in (Hussain et al., 2011), where it is discussed the main limitations of current devices is the high endpoint impedance actuators which provides issues with backdriveability as well as patients spasms (Vallery et al., 2008, Sugar et al., 2007) and as a result the patient may feel pain and discomfort. In order to create a comfortable and effective exoskeleton, Human-inspired Robotic Exoskeleton (HuREx) was developed (McDaid et al., 2013). HuREx was designed specifically for the body of each patient which improves the fit while minimising the size any discomfort for the patients. The use of PMAs (pneumatic muscle actuators) provides natural compliance while maintaining required force outputs.

In this research, a control strategy is proposed to improve the performance of the robotic exoskeleton device. A feedforward compensator which includes a hybrid model of a PMA, as well as a dynamic model of the exoskeleton device is implemented in parallel with a tuned feedback controller for robustness against modelling errors. The new control scheme was implemented in using a simulated model and the performance improvement was compared. Robustness was evaluated by inserting perturbations due to modelling inaccuracies and disturbance to the system. This new control scheme proves that the model based control system improves the performance while keeping the system robust against modelling errors and disturbances. The overall contribution of this work is improving the response time and robustness of the PMA system which will result in lower air consumption as it is a major issue for PMA systems.

2. HUMAN-INSPIRED ROBOT EXOSKELETON (HuREx) DEVICE

A robotic exoskeleton device for lower limb rehabilitation has been developed to improve the current gait rehabilitation process as shown in Fig. 1 (McDaid et al., 2013). The device can be used for more natural gait rehabilitation for neurological injuries such as stroke and traumatic brain injury as well as range of motion exercise for people with cerebral palsy. A knee joint for the lower limb rehabilitation device which consists of thigh and shank attachment has been designed and built. The design is inspired by human musculoskeletal system comprised of musculotendon units working in antagonistically about a knee joint. The device is designed to be compact and light weight and provide better fitting to the body of the patient. This should deliver more comfortable experience for the patient as well as the ease of use by the therapist.

2.1 Exoskeleton Design

There are many important factors in the design of an effective leg exoskeleton. The first factor is the shape at which can effectively transfer the torque and the forces to the leg while being safe and comfortable to the patient (not causing pressure sores on skin with long-term use). The exoskeleton device must stay on the body of a patient correctly and securely as it could move out of the position while it is in operation. This is a major issue as it could cause the device to apply incorrect forces or provide inaccurate sensor measurements. The device also needs to be comfortable to the patient as it could be worn for hours during a rehabilitation session. The impact to the patient can be minimised by elimination any pressure points on the device. HuREx device employs a custom fitting exoskeleton which is shaped specifically for the body of a patient using advanced 3D design and printing technologies. This enables the exoskeleton to be compact, easier and more comfortable for a patient while achieving the design requirements. It is also possible for a patient to wear this under their outer garments (e.g. trousers) to hide the device to reduce social stigma that may come with wearing such a device.

Fig. 1. HuREx device attached to a leg.

The HuREx exoskeleton consists of two main parts, thigh and shank which are connected by a knee joint and sliding rails. This exoskeleton acts like a human skeletal bone and will move depending on the torque applied by the antagonistic musculotendon units which is described in the next section. The two pivots and sliding rail mechanism are designed to automatically align the centre on rotation of the exoskeleton with the instantaneous centre of rotation of the knee joint (as the human knee is not an ideal rotary joint). This feature combined with the better fit of the custom exoskeleton design allow the efficient transfer of torque and power to the joint as well as providing the accurate measurement of the position (McDaid et al., 2013).

2.2 Actuation System

The actuation system of the device is inspired by the human musculoskeletal system where two muscles working in antagonistically about a joint as shown in Fig. 2. Using the model, the muscle is simulated using PMA, the tendon unit in Bowden cables, and the knee joint in pulley mechanism. The PMAs used for this device (Festo DMSP-40-300N) are 40mm diameter with a length of 300mm. They are selected based on the torque requirement at the joint and the size of the pulley used. The Bowden cables of 2.5mm were used to transfer the force from the PMAs to the exoskeleton.

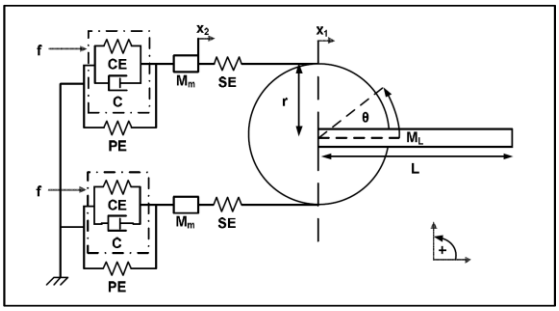

Fig. 2. The antagonistic limb joint model two antagonistically coupled Hill type muscle model actuate a single DOF limb joint (Noble et al., 2011). The model's muscles contain anatomically distinct elements: passive, parallel-elastic (PE) and serieselastic (SE) elements; an active, parallel contractile element (CE); and a parallel viscous element (C). The antagonistic mechanism has the radius, r, displacement, θ, and the length of the shank, L

3. SYSTEM MODELLING

The actual model of the rehabilitation device and PMAs are highly complex and require large computational power if they are implemented into a control system. Therefore, a simplified standard second order model was used for the modelling of the system (Chien and Huang, 2004), and a hybrid model using experimental data and dynamic modelling was used to determine the PMA characteristics (McDaid et al., 2013). The model will provide a reasonably accurate description of the system while keeping the computational requirements for the controller low.

3.1 Device Model

The overall model of the device can be expressed as the following equation (1).

$$J\ddot{\theta_k} + B\dot{\theta_k} + Gsin(\theta_k + \theta_h) = \tau \quad (1)$$

where:

J, coefficient of inertia (Assuming $J \approx I_{end}$)

where I_{end} is the moment of inertia of a rod with the axis of rotation at the end of the rod

$$J = mL^2/3 \quad (2)$$

B, combination of friction on bearing and Bowden cables

$$B = 10 \quad (3)$$

G, coefficient for the gravity component

$$G = (1/2)\,Lmg \quad (4)$$

$\theta_k(t)$, the angular position of knee joint

$\theta_h(t)$, the angular position of hip joint in sagittal plane

$\tau(t)$, the torque at the knee joint

$$\tau = (F_1 - F_2)r \tag{5}$$

$F_1(t)$ and $F_2(t)$ are the forces for each PMA

r, the radius for the pulley in metres

$$r = 0.02 \tag{6}$$

Coefficients J, B and G of the system can be found experimentally. G can be evaluated first by measuring the forces on the Bowden cable at static positions. Then J and B can be determined by back driving the system with a control system with gravitation compensation only. By plotting the position, velocity and acceleration reveals both coefficients (Tagliamonte et al., 2010). Values were estimated using this method for the following simulations.

3.2 PMA Model

There are number of researchers who have modelled their PMA as a hill-muscle type such as in (Reynolds et al., 2003). However, variability between dimensions and manufacture of PMAs result in much varying characteristics. There are also number of other models (Doumit et al., 2009, Tondu and Lopez, 2000), but a hybrid modelling strategy was proposed to accurately model the particular PMA and the dynamics of the pneumatic system used here. The method utilises empirical data to model the exact actuator type, and geometry with a physics based model for the pneumatic fluid flow. The fluid flow model was previously reported by the author in (McDaid et al., 2013).

3.3 Dynamic Model of Fluid Flow

The mass flow rate through the valve is related to the valve area, A_v, by

$$\dot{m}(P_u, P_d) = A_v \Lambda(P_u, P_d) \tag{7}$$

where

$$\Lambda(P_u, P_d) = \begin{cases} \sqrt{\frac{\gamma}{RT}\left(\frac{2}{\gamma+1}\right)^{(\gamma+1)/(\gamma-1)}} C_f P_u \\ \quad if \ \frac{P_d}{P_u} \le C_r (choked) \\ \sqrt{\frac{2\gamma}{RT(\gamma-1)}\sqrt{1-\left(\frac{P_d}{P_u}\right)^{(\gamma-1)/\gamma}}\left(\frac{P_d}{P_u}\right)^{1/\gamma}} C_f P_u \\ \quad otherwise (unchoked) \end{cases}$$

where A_v is the equivalent valve area, P_u and P_d are the upstream and downstream pressures respectively. C_f is the discharge constant and C_r is the pressure ratio that that divides the flow into choked and unchoked flow through the orifice. Note two high speed 2/2 valves operating with PWM signals are assumed to be proportional to an area of valve opening i.e. from 0-100% duty cycle relates to 0 - $A_{v(\max)}$.

The rate of change of pressure in PMA can be described by the physics based model in (8).

$$\dot{P} = \frac{\gamma R T \dot{m}}{V} - \frac{\gamma P}{V}\dot{V} \tag{8}$$

where γ is the ratio of specific heats, R is the universal gas constant, T is the gas temperature, $\dot{m}$ is the mass flow rate of air into or out of the PMA (positive models mass flowing in, negative indicates mass flowing out) and V is the volume of air inside each PMA.

The volume of the PMA used for the device was measured with varying pressure and the volume has been expressed as a function of contraction (Δx):

$$\mathrm{V} = a_0 \Delta x^3 + a_1 \Delta x^2 + a_2 \Delta x + a_3 \tag{9}$$

where the coefficients have been found to be

$a_0 = 0.0635$, $a_1 = 0.035$, $a_2 = 0.0059$, $a_3 = 0.000377$

3.4 Force-length-pressure Relationship

In order to find the relationship between the applied force, PMA length, and the pressure, an experiment was carried out with the PMA. At the experiment, the PMA was subjected to different pressure (P), and linear forces (F), and the percentage contractions of PMA (Δx) were measured. Fig. 3 shows the polynomial surface fit of force-length-pressure relationship.

Multiple polynomial orders for both contractions and forces for the fit has been tried from the first order up to fifth order. Table 1 shows the R-square values for each fit.

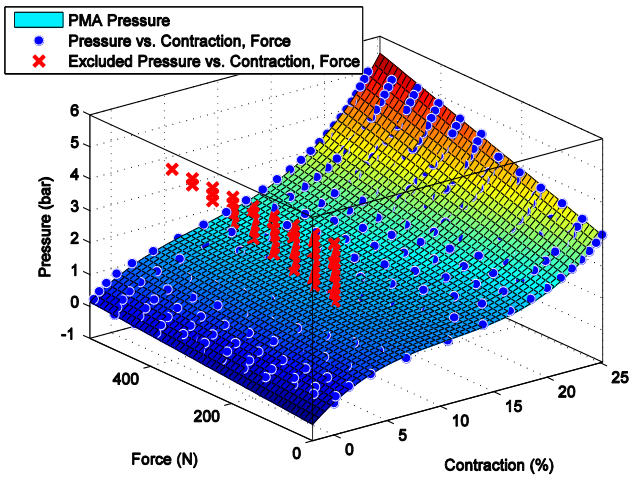

Fig. 3. Experimental results and polynomial surface fit of the pressure as a function of force and contraction of PMA

Table 1. R^2 values of polynomial fit

		Polynomial Order (Contraction)				
Polynomial Order (Force)		1	2	3	4	5
	1	0.9202	0.9756	0.9978	0.998	0.9988
	2	0.9398	0.9758	0.9981	0.9985	0.9993
	3	0.9401	0.9766	0.9981	0.9985	0.9994
	4	0.9404	0.9768	0.9985	0.9985	0.9994
	5	0.9404	0.9769	0.9985	0.9985	0.9994

By using the results, third order for the contraction and the first order for the force were chosen as the optimal point, since it provided the balance between the fit accuracy (R-square: 0.9978) and the complexity of the polynomial. The final mathematical model of the PMA is the following.

$$P(\Delta x, F) = p_{00} + p_{10}\Delta x + p_{01}F + p_{20}\Delta x^2 + p_{11}\Delta xF + p_{30}\Delta x^3 + p_{21}\Delta x^2\mathrm{F} \quad (10)$$

Coefficients (with 95% confidence bounds):
p_{00} = 0.025 (-0.01198, 0.06198)
p_{10} = 0.2181 (0.2071, 0.229)
p_{01} = 0.001016 (0.0009157, 0.001116)
p_{20} = -0.01748 (-0.01835, -0.0166)
p_{11} = -4.796e-05 (-6.867e-05, -2.726e-05)
p_{30} = 0.000533 (0.0005117, 0.0005542)
p_{21} = 7.474e-06 (6.641e-06, 8.306e-06)

where p_x are coefficients, P is the pressure in bar (100kPa), F is the force in Newton, and Δx in the contraction of PMA in %.

4. CONTROL SYSTEM DESIGN

A control system was designed to operate the rehabilitation device using the National Instrument CompactRIO running at 100Hz to achieve real-time control. A simple closed-loop PID control was created for an initial trajectory tracking experiment as a benchmark. However, highly non-linear characteristic nature of PMA and the exoskeleton system caused an inaccurate and slow response of the device. As the result, model based control system was proposed to improve the speed and the accuracy of the control system.

4.1 Closed-loop PID Control

In order to test the device, a trajectory tracking simple impedance control system was designed. The system schematic is shown in Fig. 4. This impedance controller, which is essentially a PD controller, takes the angular position and velocity errors and determines the required torque output of the exoskeleton at the knee joint, then the required force outputs for each PMA. A nominal force was set for both PMAs in order to keep both cables in tension, so the desired forces were calculated using (11).

$$F_{di} = \tau_d/r + F_{ni}, (i=1,2) \quad (11)$$

where τ_d is the desired torque, r is the pulley radius, and F_n is the nominal force.

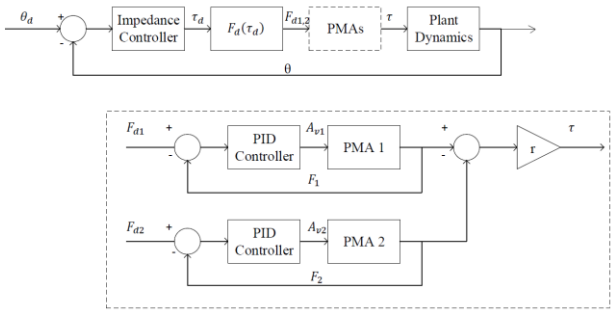

Fig. 4. Closed-loop PID control schematics

The force output of PMA is controlled using a simple closed-loop PID controller. However, PID controller is unsuited for controlling force output of PMA which is inherently non-linear. Therefore, this controller was only used for the initial testing.

The PID gains are tuned iteratively to determine a good overall response for the non-linear system.

4.2 Model based Feedforward Controller

With the aim of developing a stable, accurate and fast control system, mathematical model based control strategy was applied. Fig. 5 shows the overall schematics of the new system. The system utilises two feedforward controller for each PMA. Addition of feedforward control improves performance over a simple feedback control system by accurately predicting the exact controller requirement from the model (Oosting, 1987).

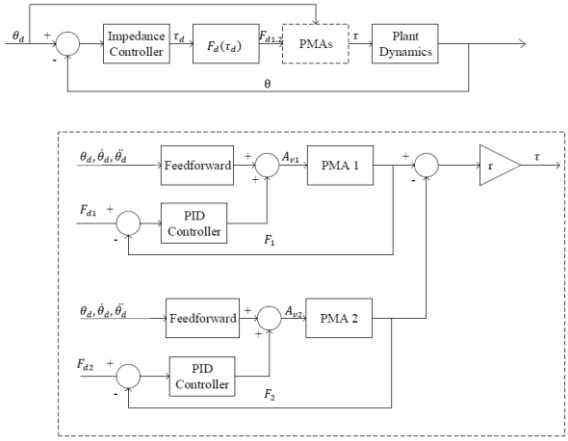

Fig. 5. Schematics of model based feedforward control parallel with closed-loop PID control

The controllers calculate the valve area for each PMA, A_v from the reference trajectory, θ_d using the model of the system. A closed-loop feedback loop works in parallel to handle any disturbance.

The output of the feedforward controller is the valve area for each PMA which can be found by rearranging (7).

$$A_v = \frac{\dot{m}(P_u, P_d)}{\Lambda(P_u, P_d)} \quad (12)$$

where $\dot{m}$ can be found by rearranging (8).

$$\dot{m} = \frac{\dot{P}V}{\gamma RT} + \frac{P\dot{V}}{RT} \quad (13)$$

where $\dot{V}$ and $\dot{P}$ can be calculated by differentiating (9) and (10) respectively.

Differentiating (10) requires F and $\dot{F}$ which are found using (1) and (5).

The result of these substitution is an expressing for A_v as a function of Δx, $\Delta\dot{x}$ *and* $\Delta\ddot{x}$.

Δx for each PMA are related to angular position of knee joint, θ and can be found by analysing the geometry of the pulley.

$$\Delta x = x_i + (\theta + 45)r \qquad (14)$$

where $x_i$is the initial contraction at resting position, and r is the pulley radius.

5. RESULTS

Simulations for controllers were carried out to verify their performance. The system model of the device was used for both simple trajectory tracking control system and the control system with model based feedforward path. Simulation experiments with sine wave reference trajectory were carried out to see the speed and accuracy of the control system. The sine wave has the period of 20s and the amplitude of 10°. The trajectories of only the first three cycles are shown in this result as the cycle continues consistently due to the perfect simulation environment. Fig. 6 shows the reference trajectory and the actual trajectory of the system with closed-loop PID controls. Fig. 7 shows the same experiment with model-based feedforward control system. The graphs show that the both control system achieved very accurate trajectory tracking results, as they used the ideal models of the system and perfect environment without any disturbances.

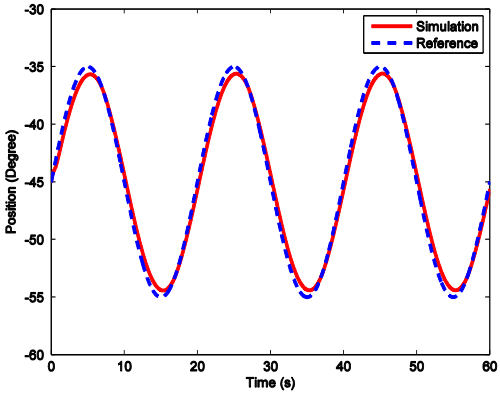

Fig. 6. Trajectory tracking result of closed-loop PID control system

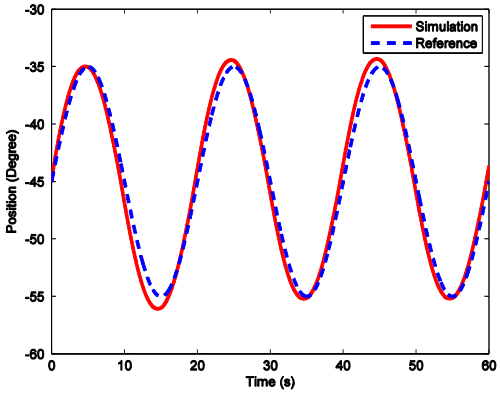

Fig. 7. Trajectory tracking result of feedforward control system

Another simulation was carried out with a system with noise on position sensor output. Fig. 8 shows the trajectory tracking result of closed-loop system, and Fig. 9 shows the same experiment with feedforward system. The closed-loop only system was severely affected by the noise while the system with feedforward path has continued to achieve accurate trajectory tracking result. This is due to the model in the feedforward loop is undertaking most of the control action while the controller in the closed-loop system solely relies on the sensor reading to determine the output.

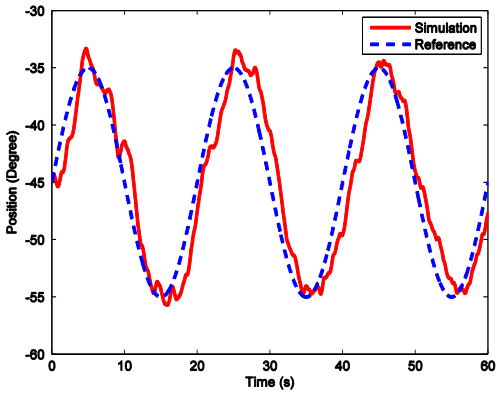

Fig. 8. Trajectory tracking result of closed-loop PID control system with disturbance

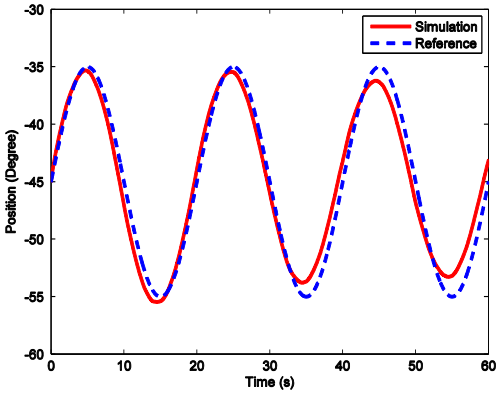

Fig. 9. Trajectory tracking result of feedforward control system with disturbance

Further simulations were carried out on the feedforward system with varying plant characteristics: mass and the friction coefficient. The values ware changed as much as +/- 50% to simulate modelling error. The results of these experiments showed the controller achieving consistent tracking performance with no noticeable performance decrement in comparison with a ‘perfect’ model proving the robustness of the designed control system.

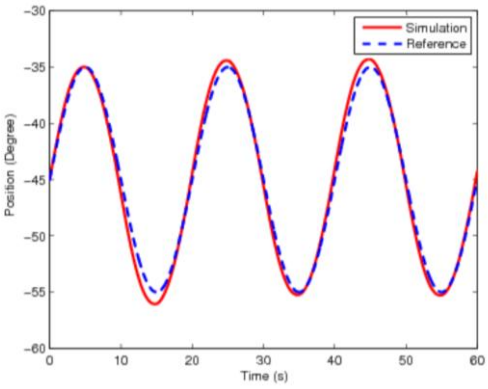

Fig. 11. Trajectory tracking result of feedforward control system with +50% mass of shank

6. DISCUSSIONS AND CONCLUSIONS

A model for Human-inspired Robotic Exoskeleton device and Festo PMA used for the device has been developed successfully using theories and experiments. The model was able to describe the system reasonably accurately while keeping it simple.

A simple closed-loop feedback control and another control system using above models were developed for HuREx device. The model based control system was used to improve the performance of the system which is highly non-linear.

Simulations of the system with the simple feedback control and the model based control was carried out using Simulink. The trajectory tracking results shows a clear improvement on the speed and accuracy of the model based control system on the rehabilitation device.

The newly developed control system has proven to be very promising. However, the performance on the actual system is untested and the unclear to whether the accuracy of the simulation and the models hold true in the real world.

7. ACKNOWLEDGEMENT

The authors gratefully acknowledge the financial support provided by the Auckland Medical Research Foundation.

REFERENCES

Chien, M.-C. & Huang, A.-C. 2004. Adaptive Impedance Control of Robot Manipulators based on Function Approximation Technique. *Robotica,* 22**,** 395-403.

Doumit, M., Fahim, A. & Munro, M. 2009. Analytical Modeling and Experimental Validation of the Braided Pneumatic Muscle. *Robotics, IEEE Transactions on,* 25**,** 1282-1291.

Healthsouth. *HealthSouth's AutoAmbulator®* [Online]. Available: http://www.healthsouth.com/en/ [Accessed 9 April 2013].

Hussain, S., Xie, S. Q. & Liu, G. 2011. Robot assisted treadmill training: Mechanisms and training strategies. *Medical Engineering & Physics,* 33**,** 527-533.

Mcdaid, A., Kora, K., Xie, S., Lutz, J. & Battley, M. Human-inspired robotic exoskeleton (HuREx) for lower limb rehabilitation. Mechatronics and Automation (ICMA), 2013 IEEE International Conference on, 4-7 Aug. 2013 2013. 19-24.

Noble, F. K., Potgieter, J. & Xu, W. L. Modelling and simulations of a central pattern generator controlled, antagonistically actuated limb joint. Systems, Man, and Cybernetics (SMC), 2011 IEEE International Conference on, 9-12 Oct. 2011 2011. 2898-2903.

Oosting, K. W. 1987. Simulation of control strategies for a two degree-of-freedom lightweight flexible robotic arm.

Perry, J., Garrett, M., Gronley, J. K. & Mulroy, S. J. 1995. Classification of Walking Handicap in the Stroke Population. *Stroke,* 26**,** 982-989.

Reynolds, D. B., Repperger, D. W., Phillips, C. A. & Bandry, G. 2003. Modeling the Dynamic Characteristics of Pneumatic Muscle. *Annals of Biomedical Engineering,* 31**,** 310-317.

Riener, R., Lunenburger, L., Jezernik, S., Anderschitz, M., Colombo, G. & Dietz, V. 2005. Patient-cooperative strategies for robot-aided treadmill training: first experimental results. *Neural Systems and Rehabilitation Engineering, IEEE Transactions on,* 13**,** 380-394.

Sugar, T. G., Jiping, H., Koeneman, E. J., Koeneman, J. B., Herman, R., Huang, H., Schultz, R. S., Herring, D. E., Wanberg, J., Balasubramanian, S., Swenson, P. & Ward, J. A. 2007. Design and Control of RUPERT: A Device for Robotic Upper Extremity Repetitive Therapy. *Neural Systems and Rehabilitation Engineering, IEEE Transactions on,* 15**,** 336-346.

Tagliamonte, N. L., Formica, D., Scorcia, M., Campolo, D. & Guglielmelli, E. Force control of a robot for wrist rehabilitation: Towards coping with human intrinsic constraints. Intelligent Robots and Systems (IROS), 2010 IEEE/RSJ International Conference on, 18-22 Oct. 2010 2010. 4384-4389.

Tilson, J. K., Sullivan, K. J., Cen, S. Y., Rose, D. K., Koradia, C. H., Azen, S. P., Duncan, P. W. & For the Locomotor Experience Applied Post Stroke Investigative, T. 2010. Meaningful Gait Speed Improvement During the First 60 Days Poststroke: Minimal Clinically Important Difference. *Physical Therapy,* 90**,** 196-208.

Tondu, B. & Lopez, P. 2000. Modeling and control of McKibben artificial muscle robot actuators. *Control Systems, IEEE,* 20**,** 15-38.

Vallery, H., Veneman, J., Van Asseldonk, E., Ekkelenkamp, R., Buss, M. & Van Der Kooij, H. 2008. Compliant actuation of rehabilitation robots. *Robotics & Automation Magazine, IEEE,* 15**,** 60-69.

Veneman, J. F., Kruidhof, R., Hekman, E. E. G., Ekkelenkamp, R., Van Asseldonk, E. H. F. & Van Der Kooij, H. 2007. Design and Evaluation of the LOPES Exoskeleton Robot for Interactive Gait Rehabilitation. *Neural Systems and Rehabilitation Engineering, IEEE Transactions on,* 15**,** 379-386.

Wade, D. T. & Hewer, R. L. 1987. Functional abilities after stroke: measurement, natural history and prognosis. *Journal of Neurology, Neurosurgery & Psychiatry,* 50**,** 177-182.